Practical Assessment of Real-Time Impact Point Estimators for Smart Weapons

Article *in* Journal of Aerospace Engineering · January 2010

DOI: 10.1061/(ASCE)AS.1943-5525.0000044

3 authors, including:

Mark Costello
Georgia Institute of Technology
192 PUBLICATIONS **3,177** CITATIONS

Practical Assessment of Real-Time Impact Point Estimators for Smart Weapons

Frank Fresconi[1]; Gene Cooper[2]; and Mark Costello[3]

Abstract: There are numerous ways to estimate the trajectory and subsequent impact point of a projectile. Some complex methods are highly accurate and require a lot of input data while others are fairly trivial and less accurate but require minimal input data. Projectile impact point predictors (IPPs) have three primary error sources: model error, parameter error, and initial state error. While model error typically shrinks as model complexity increases, parameter and initial state errors grow with increasing model complexity. Since all input data feeding an IPP are uncertain to some level, the ideal IPP for an overall situation is not clear cut by any means. This paper examines several different projectile IPPs that span the range of complex nonlinear rigid projectile models to simple vacuum point mass models with the intent to better understand relative merits of each algorithm in relation to the other algorithms and as a function of parameter uncertainty and initial state error. Monte Carlo simulation is employed to compute impact point statistics as a function of the range to the target for an indirect fire 155-mm spin stabilized round. For this specific scenario, results indicated neglecting physical phenomena in the formulation of the equations of motion can degrade impact point prediction, especially early in the flight. Adding uncertainty to the parameters and states induces impact point errors that dominate model error contributions. Impact point prediction errors scaled linearly with parameter and state errors. All IPPs investigated converged to the actual impact point as the time at which the estimate took place approached the time of impact.

DOI: 10.1061/(ASCE)AS.1943-5525.0000044

CE Database subject headings: Weapons; Monte Carlo method; Models; Errors.

Author keywords: Impact point predictors; Monte Carlo; Model error.

Introduction

One typical characteristic of smart projectiles is relatively low control authority. For example, it is common for control actuators on a smart projectile to modify the impact point of an indirect fire shot by 200 m at a range of 20,000 m. For this reason, control of smart projectiles is sometimes called "ballistic nudging." Since control authority for smart projectiles is usually small, flight control systems must efficiently move the bullet in-flight to its intended impact point. To this end, projectile impact point predictors (IPPs) are often embedded inside the flight control system of smart weapons to project the effect of control action on the impact point with the end goal of minimizing control effort (Burchett and Costello 2002).

At the core of any projectile trajectory calculator is the solution of a set of dynamic equations of motion, either analytic or numeric. These dynamic models are driven by a set of input parameters such as mass properties and aerodynamic coefficients, as well as the initial state of the projectile which depending on the dynamic model can include initial position, orientation, and velocity. Because model parameters and the initial state of the projectile are uncertain to some degree, each IPP will have three major sources of error: model error, parameter error, and initial state error. Model error arises from the fact that no trajectory model can perfectly predict physical reality. Of course, some trajectory models are better than others in this sense. Parameter errors stem from the fact there will always be a mismatch with parameter values used in the trajectory calculator and the physical system. Initial state errors arise from the fact that the trajectory calculator requires the initial state of the projectile to propagate the solution to the impact area. The initial state is measured by sensors or estimated through an observer leading to errors between the trajectory calculator and the physical projectile. An ideal projectile IPP is sufficiently accurate for its intended purpose, computationally efficient so impact point estimates can be performed in real time on a microprocessor and can be driven by a minimal data set.

Many different trajectory calculators are available with varying levels of fidelity and data requirements. These methods loosely fall into three categories: rigid body, modified point mass (MPM), and point mass methods. Rigid body methods assume that the projectile is a rigid body that possesses three position and three orientation degrees of freedom. These models require mass and inertia properties, extensive aerodynamic coefficient data, and 12 initial state conditions. As the name suggests, point mass methods assume that the projectile is a point mass that possesses three position degrees of freedom. These models require mass, aerodynamic drag data, and six initial state conditions. The MPM model assumes that the projectile is a point mass, but the roll

[1]Mechanical Engineer, Aerodynamics Branch, U.S. Army Research Laboratory, Aberdeen Proving Ground, MD 21005.

[2]Research Physicist, Aerodynamics Branch, U.S. Army Research Laboratory, Aberdeen Proving Ground, MD 21005 (corresponding author).

[3]Sikorsky Associate Professor, School of Aerospace Engineering, Georgia Institute of Technology, Atlanta, GA 30332.

Note. This manuscript was submitted on December 30, 2008; approved on January 13, 2010; published online on January 28, 2010. Discussion period open until June 1, 2011; separate discussions must be submitted for individual papers. This paper is part of the ***Journal of Aerospace Engineering***, Vol. 24, No. 1, January 1, 2011. ©ASCE, ISSN 0893-1321/2011/1-1–11/$25.00.

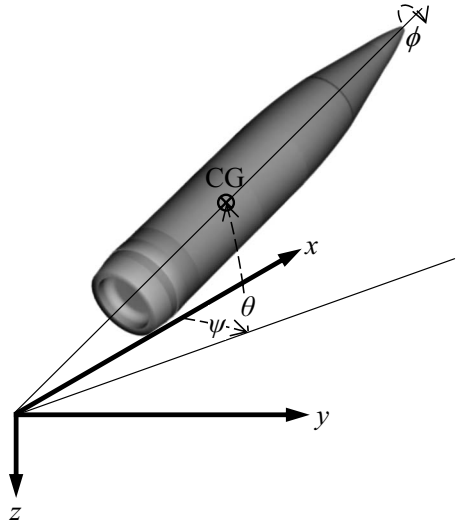

Fig. 1. Illustration of coordinate system and Euler angles

dynamic equation is appended to the model along with side force to better replicate cross range of spin stabilized projectiles. It has data requirements between the rigid body and point mass models. While rigid body projectile models are considered the most accurate with the least model error, they generally also require the most input data and as such have the most parameter and initial state error. At the other end of the spectrum is the point mass model without aerodynamics. This model is generally considered the least accurate model with the largest associated model error. However, it also requires the least number of input parameters leading to the lowest parameter and initial state error. Thus, depending on knowledge of an optimal projectile IPP must balance model error with parameter and initial state error.

This paper examines the merits of different smart weapon IPPs and creates a methodology to identify an overall ideal smart weapon IPP for a given application. The effects of all major sources of parametric and initial state uncertainty are included in the analysis. IPP accuracy is assessed from a statistical perspective using the extensive Monte Carlo simulation using all candidate IPPs. Results are presented in terms of mean and standard deviation of the impact point prediction and parametric trade studies are reported that vary the range to the target, the uncertainty of mass properties, the uncertainty of aerodynamic properties, and the level of measurement errors.

IPPs

Seven different IPPs are considered in this effort. Equations of motion, required parameters (such as mass), and initial states (such as muzzle velocity) make up an IPP. The equations of motion and associated parameters and input states will be briefly presented for each IPP (McCoy 1999). A North-East-Down coordinate system with the origin at the launch point was employed for each IPP. Fig. 1 illustrates the projectile with center of gravity (CG) in this coordinate system along with orientations of the Euler angles (ϕ,θ,ψ). All calculations were performed with a symmetric projectile in a standard atmosphere with no atmospheric winds.

The most complex representation of projectile motion is the six degrees-of-freedom (6DOF) model. The 6DOF model in the no-roll reference frame is given in Eqs. (1)–(4). The dot notation signifies a derivative in time (t). Twelve states $(x,y,z,\phi,\theta,\psi,\tilde{u},\tilde{v},\tilde{w},\tilde{p},\tilde{q},\tilde{r})$ comprise the 6DOF model. This set of coupled nonlinear ordinary differential equations requires initial states, acceleration of gravity, atmospheric density and sound speed, mass, inertia tensor (axial and transverse inertia for symmetric projectiles), location of CG, diameter, and tables of aerodynamic coefficients as a function of the Mach number to calculate projectile dynamics

$$\begin{Bmatrix}\dot{x}\\ \dot{y}\\ \dot{z}\end{Bmatrix}=\begin{bmatrix}c_\theta c_\psi & -s_\psi & s_\theta c_\psi\\ c_\theta s_\psi & c_\psi & s_\theta s_\psi\\ -s_\theta & 0 & c_\theta\end{bmatrix}\begin{Bmatrix}\tilde{u}\\ \tilde{v}\\ \tilde{w}\end{Bmatrix} \tag{1}$$

$$\begin{Bmatrix}\dot{\phi}\\ \dot{\theta}\\ \dot{\psi}\end{Bmatrix}=\begin{bmatrix}1 & 0 & t_\theta\\ 0 & 1 & 0\\ 0 & 0 & 1/c_\theta\end{bmatrix}\begin{Bmatrix}\tilde{p}\\ \tilde{q}\\ \tilde{r}\end{Bmatrix} \tag{2}$$

$$\begin{Bmatrix}\dot{\tilde{u}}\\ \dot{\tilde{v}}\\ \dot{\tilde{w}}\end{Bmatrix}=\begin{Bmatrix}\tilde{X}/m\\ \tilde{Y}/m\\ \tilde{Z}/m\end{Bmatrix}+\begin{Bmatrix}\tilde{r}\tilde{v}-\tilde{q}\tilde{w}\\ -t_\theta\tilde{r}\tilde{w}-\tilde{r}\tilde{u}\\ \tilde{q}\tilde{u}+t_\theta\tilde{r}\tilde{v}\end{Bmatrix} \tag{3}$$

$$\begin{Bmatrix}\dot{\tilde{p}}\\ \dot{\tilde{q}}\\ \dot{\tilde{r}}\end{Bmatrix}=[I]^{-1}\left(\begin{Bmatrix}\tilde{L}\\ \tilde{M}\\ \tilde{N}\end{Bmatrix}\begin{bmatrix}0 & -\tilde{r} & \tilde{q}\\ \tilde{r} & 0 & \tilde{r}t_\theta\\ -\tilde{q} & -\tilde{r}t_\theta & 0\end{bmatrix}[I]\begin{Bmatrix}\tilde{p}\\ \tilde{q}\\ \tilde{r}\end{Bmatrix}\right) \tag{4}$$

The linear theory of projectile motion is a closed-form solution that is a simplification of the 6DOF model. Linear theory provides reasonably accurate representations of flat fire and short time of flight trajectories. Modified linear theory (MLT) was developed to accommodate higher quadrant elevation and longer time of flight trajectories (Hainz and Costello 2005). The equations of motion for MLT are given in Eqs. (5)–(16). The prime notation denotes a derivative in space (s). MLT needs 12 initial states $(x',y',z',\phi',\theta',\psi',V',\tilde{v}',\tilde{w}',\tilde{p}',\tilde{q}',\tilde{r}')$. Parameters required by MLT include acceleration of gravity, atmospheric density and sound speed, mass, axial inertia, transverse inertia, location of CG, diameter, and almost the same set of aerodynamic coefficients used in the 6DOF

$$x'=c_\theta D \tag{5}$$

$$y'=c_\theta D\psi+\frac{D}{V}\tilde{v} \tag{6}$$

$$z'=-Ds_\theta+\frac{Dc_\theta}{V}\tilde{w} \tag{7}$$

$$\phi'=\frac{D}{V}\tilde{p} \tag{8}$$

$$\theta'=\frac{D}{V}\tilde{q} \tag{9}$$

$$\psi'=\frac{D}{Vc_\theta}\tilde{r} \tag{10}$$

$$V'=-\frac{\pi\rho D^3}{8m}C_{X0}V-\frac{Dg}{V}s_\theta \tag{11}$$

$$\tilde{v}' = -\frac{\pi\rho D^3}{8m} C_{NA}\tilde{v} - D\tilde{r} \tag{12}$$

$$\tilde{w}' = -\frac{\pi\rho D^3}{8m} C_{NA}\tilde{w} + D\tilde{q} + \frac{Dgc_\theta}{V} \tag{13}$$

$$\tilde{p}' = \frac{\pi\rho V D^4}{8I_{XX}} C_{DD} + \frac{\pi\rho D^5}{16I_{XX}} C_{LP}\tilde{p} \tag{14}$$

$$\tilde{q}' = \frac{\pi\rho D^4 R_{MCM}}{16I_{YY}V} C_{YPA}\tilde{p}\tilde{v} + \frac{\pi\rho D^3 R_{MCP}}{8I_{YY}} C_{NA}\tilde{w} + \frac{\pi\rho D^5}{16I_{YY}} C_{MQ}\tilde{q} - \frac{I_{XX}D}{I_{YY}V}\tilde{p}\tilde{r}_q \tag{15}$$

$$\tilde{r}' = -\frac{\pi\rho D^3 R_{MCP}}{8I_{YY}} C_{NA}\tilde{v} + \frac{\pi\rho D^4 R_{MCM}}{16I_{YY}V} C_{YPA}\tilde{p}\tilde{w} + \frac{I_{XX}D}{I_{YY}V}\tilde{p}\tilde{q} + \frac{\pi\rho D^5}{16I_{YY}} C_{MQ}\tilde{r} \tag{16}$$

The MPM model was developed to rapidly predict the fire control solution for artillery systems (Lieske and Reiter 1966; Cooper et al. 1997). Artillery drifts in the cross-range direction due to yaw of repose. Yaw of repose is a complex phenomenon produced by the interaction of spin, gravity, and aerodynamics. The MPM model, presented in Eqs. (17)–(20), includes terms for the rotational degree of freedom about the spin axis and yaw of repose. Initial states necessary for MPM calculations are the position, velocity, and spin rate $(x, y, z, \dot{x}, \dot{y}, \dot{z}, \dot{\phi})$. The acceleration of gravity, atmospheric density and sound speed, mass, axial inertia, location of CG, diameter, aerodynamic coefficients of axial force, normal force, Magnus moment, and roll damping moment are shown. Here

$$\ddot{x} = \left\{ -\left[\frac{\pi\rho V D^2}{8m}\right]\left[C_{X0} + \left(C_{X2} + C_{NA} - \frac{1}{2}C_{X0}\right)|\alpha_r|^2 \right]\right\}\dot{x} + \frac{1}{(1+h_a)}\left[\frac{h_L(-g\dot{y})}{(1-h_M)V}\right] \tag{17}$$

$$\ddot{y} = \left\{ -\left[\frac{\pi\rho V D^2}{8m}\right]\left[C_{X0} + \left(C_{X2} + C_{NA} - \frac{1}{2}C_{X0}\right)|\alpha_r|^2 \right]\right\}\dot{y} + \frac{1}{(1+h_a)}\left[\frac{h_L(-g\dot{x})}{(1-h_M)V}\right] \tag{18}$$

$$\ddot{z} = \left\{ \frac{h_a g\dot{z}}{(1-h_a)V^2} - \left[\frac{\pi\rho V D^2}{8m}\right]\left[C_{X0} + \left(C_{X2} + C_{NA} - \frac{1}{2}C_{X0}\right) \times|\alpha_r|^2 \right]\right\}\dot{z} + \frac{g}{(1+h_a)} \tag{19}$$

$$\ddot{\phi} = -\left(\frac{\pi\rho V^2 D^2}{8I_{XX}}\right) C_{LP}\left(\frac{\dot{\phi}D}{2V}\right) \tag{20}$$

The equations of motion shown in Eqs. (21)–(23) apply to a family of point mass IPPs. Initial states for all point mass IPPs are position and velocity $(x, y, z, \dot{x}, \dot{y}, \dot{z})$. The full point mass (FPM) IPP updates the atmospheric density and zero-yaw axial force coefficient as the projectile flies. The simple point mass (SPM) IPP uses the density and zero-yaw axial force coefficient at launch. Besides zero-yaw axial force coefficient, both FPM and SPM require acceleration of gravity, atmospheric density and sound speed, mass, and diameter. The vacuum point mass (VPM) does not include aerodynamics (C_{X0}=0) and therefore only treats gravitational forces acting on the projectile. Here

$$\ddot{x} = -\frac{\pi\rho D^2 C_{XO} V}{8m}\dot{x} \tag{21}$$

$$\ddot{y} = -\frac{\pi\rho D^2 C_{XO} V}{8m}\dot{y} \tag{22}$$

$$\ddot{z} = -\frac{\pi\rho D^2 C_{XO} V}{8m}\dot{z} + g \tag{23}$$

The hybrid point mass (HPM) IPP is so called because an updated drag estimate is used in a vacuum-type equation of motion. The drag per unit mass in three directions is assessed by Eqs. (24)–(26). The acceleration in the z-direction is then placed in Eq. (27) to estimate the time-of-flight remaining (t_{go}). Eqs. (27) and (28) are used to calculate the impact location in x and y for this t_{go}. HPM requires the same initial states $(x, y, z, \dot{x}, \dot{y}, \dot{z})$ and parameters $(g, \rho, c, m, D, C_{X0})$ as FPM and SPM. Here

$$\ddot{x} = -\frac{\pi\rho D^2 C_{XO} V^2}{8m}\cos\theta_v \cos\varphi_v \tag{24}$$

$$\ddot{y} = -\frac{\pi\rho D^2 C_{XO} V^2}{8m}\cos\theta_v \sin\varphi_v \tag{25}$$

$$\ddot{z} = g + \frac{\pi\rho D^2 C_{XO} V^2}{8m}\sin\theta_v \tag{26}$$

$$t_{go} = -\frac{\dot{z} - \sqrt{\dot{z}^2 - 2\ddot{z}z}}{\ddot{z}} \tag{27}$$

$$x_i = x + \dot{x}t_{go} + \frac{1}{2}\ddot{x}t^2 \tag{28}$$

$$y_i = y + \dot{y}t_{go} + \frac{1}{2}\ddot{y}t^2 \tag{29}$$

Table 1 summarizes the necessary states and parameters for each of the seven IPPs investigated in this effort. Closed-form solutions exist for the MLT, FPM, SPM, HPM, and VPM IPPs. A high speed of calculation is associated with a closed-form solution. The speed of calculation is important when implementing a given IPP real time on a digital signal processor in the guidance and control of a precision munition.

Results

A 155-mm artillery projectile was selected as the test bed. Physical characteristics are supplied in Table 2. Aerodynamics consisted of coefficients of axial force, normal force, Magnus force, pitching moment, pitch damping moment, roll damping moment, and Magnus moment. These physical properties and aerodynamics are typical of a spin-stabilized indirect fire round.

Baseline trajectories were generated from the 6DOF model. The projectile emerged from the muzzle with a velocity of 656.8

Table 1. Summary of IPP Required States and Parameters

IPP	States	Parameters
6DOF	$x,y,z,\phi,\theta,\psi,\tilde{u},\tilde{v},\tilde{w},\tilde{p},\tilde{q},\tilde{r}$	$g,\rho,c,m,D,I_{XX},I_{YY},CG,C_{X0},C_{X2},C_{NA},C_{YPA},C_{MA},C_{MQ},C_{NPA},C_{DD},C_{LP}$
MLT	$x',y',z',\phi',\theta',\psi',V',\tilde{v}',\tilde{w}',\tilde{p}',\tilde{q}',\tilde{r}'$	$g,\rho,c,m,D,I_{XX},I_{YY},CG,C_{X0},C_{NA},C_{MA},C_{MQ},C_{NPA},C_{DD},C_{LP}$
MPM	$x,y,z,\dot{x},\dot{y},\dot{z},\dot{\phi}$	$g,\rho,c,m,D,I_{XX},CG,C_{X0},C_{X2},C_{NA},C_{NPA},C_{LP}$
FPM	$x,y,z,\dot{x},\dot{y},\dot{z}$	g,ρ,c,m,D,C_{X0}
SPM	$x,y,z,\dot{x},\dot{y},\dot{z}$	g,ρ,c,m,D,C_{X0}
HPM	$x,y,z,\dot{x},\dot{y},\dot{z}$	g,ρ,c,m,D,C_{X0}
VPM	$x,y,z,\dot{x},\dot{y},\dot{z}$	g

m/s and spin rate of 1332.0 rad/s. The quadrant elevation was 20° and launch disturbances $(\tilde{v},\tilde{w},\tilde{q},\tilde{r})$ were set to zero.

The baseline flight dynamics at 20° quadrant elevation are provided in Fig. 2. The projectile flew almost 15 km down range and reached a peak altitude over 1.5 km. The effect of yaw of repose to induce a yaw angle is seen in the projectile drifting to the right (when viewed from behind) by over 100 m in Fig. 2(a). The flight spanned supersonic to the transonic Mach numbers. The angle of attack behavior illustrates the yaw of repose (negative β) and effect of nonlinear Magnus moment. The coning motion of approximately 3° total angle of attack is a limit cycle that occurs for about the final 20% of the flight.

Table 2. Projectile Physical Properties

M (kg)	I_{XX} (kg m^2)	I_{YY} (kg m^2)	CG from nose (m)	D (m)
46.72	0.1586	1.692	0.5631	0.1547

The 6DOF model baseline flight dynamics served as ground truth by providing the states and the actual impact location from which all IPPs were evaluated. At chosen instants along the trajectory, projectile states from the baseline 6DOFsimulation were used to obtain initial states in the IPP algorithms.

To understand the inherent ability of a given IPP to represent physical reality, each IPP algorithm was performed with perfect initial state and parameter information. Thus, the effect of dynamic model errors was isolated. A normalized time of flight (T^*) was obtained by dividing the time of flight by the time of impact. This normalized time was chopped into 40 equal divisions and the baseline 6DOF states and parameters were used in each IPP to predict the impact point. At each time at which the impact point was predicted, the down-range (μ_X), cross-range (μ_Y), and radial (μ_R) distances from the baseline impact location were captured.

These data (μ_X,μ_Y,μ_R) are shown for a 20° quadrant elevation in Fig. 3 for the seven IPPs. The 6DOF IPP predicts a perfect impact point because the truth model has the same 6DOF equa-

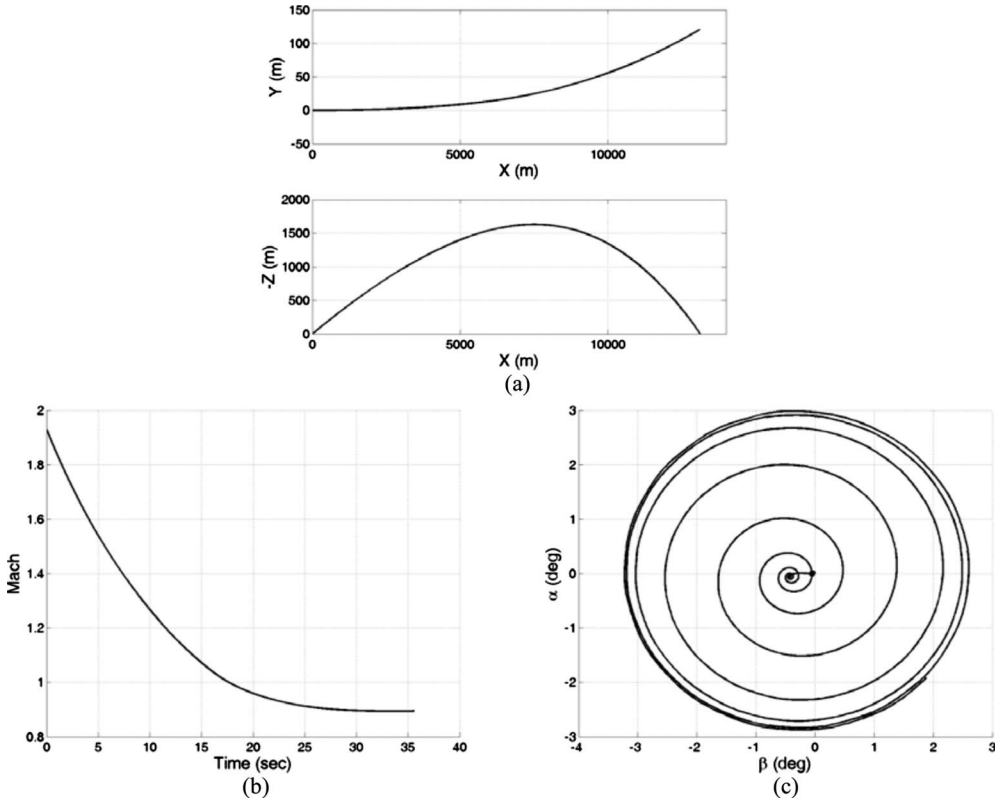

Fig. 2. Flight dynamics of the artillery projectile at 20° quadrant elevation: (a) trajectory; (b) Mach number history; and (c) angle of attack behavior

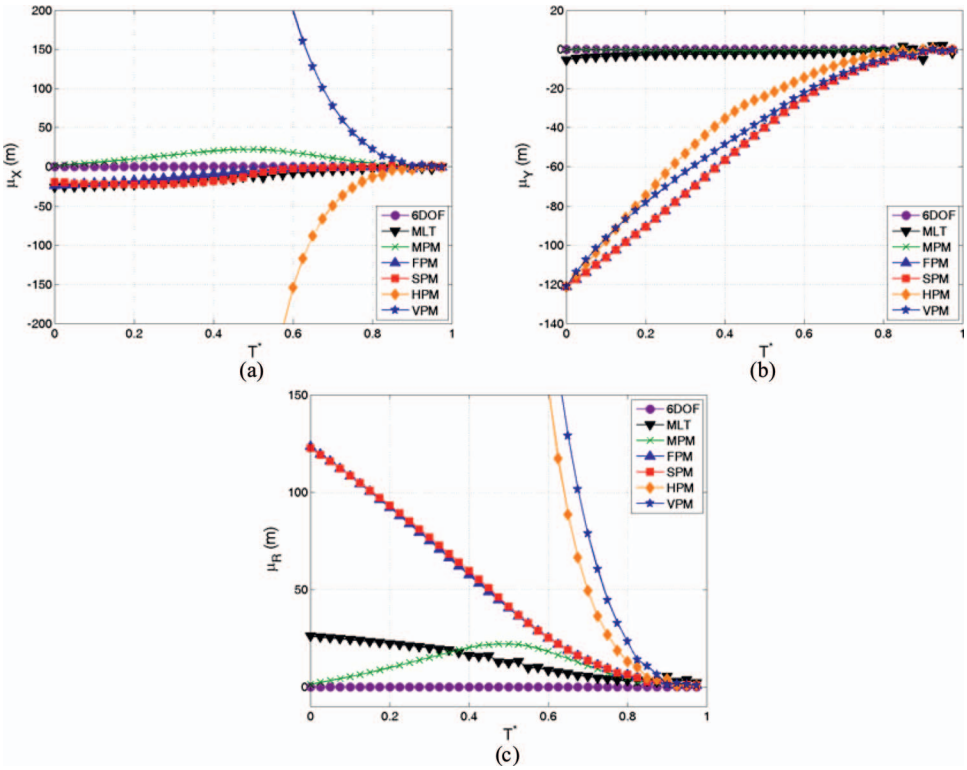

Fig. 3. (Color) Mean of impact point prediction for 20° quadrant elevation and perfect parameters and initial states: (a) down-range direction; (b) cross-range direction; and (c) radial direction

tions of motion and the initial states and parameters have no associated errors. Errors evidenced the results in Fig. 3 for all IPPs other than the 6DOF are solely due to modeling deficiencies (assuming the 6DOF model as truth).

Down-range impact is underpredicted by the MLT, FPM, and SPM IPPs by about 25 m at $T^*=0$ and improves as $T^* \rightarrow 1$. Range is underpredicted by the FPM and SPM IPPs even though yaw drag is not included in the point mass equations of motion. The updating of atmospheric density and zero-yaw axial force for the FPM IPP does not appreciably increase down-range impact prediction over the SPM IPP. MPM performance decreases by about 20 m from launch ($T^*=0$) to apogee (approximately $T^*=0.5$); possibly due to the yaw of repose not being appropriately accounted for in the MPM model. The down-range model errors of the MLT, MPM, FPM, and SPM IPPs for this case have a similar order of magnitude throughout the flight. Down-range impact is underestimated by more than 150 m for $T^*<0.6$ for the HPM IPP because t_{go} is underpredicted due to an overpredicted deceleration in the z-direction. Neglecting drag is shown in the VPM results to overestimate the down-range impact point by more than 200 m for $T^*<0.6$. Down-range performance of all IPPs improves as $T^* \rightarrow 1$.

The cross-range results of Fig. 3(b) are quickly broken into IPPs that account for projectile drift and those that do not. The 6DOF, MLT, and MPM have less than 10 m of cross-range error throughout the flight due to including the effect of yaw of repose. Cross range is predicted to be less than 1 m for the entire flight by the MPM IPP. Past $T^*=0.8$, the MLT cross-range predictions jump around by a few meters. This is likely due to the action of the limit cycle seen for the final 20% of the flight in Fig. 2(c). The fully nonlinear behavior of the Magnus moment in the 6DOF is not completely captured in the MLT equations of motion. The point mass derivatives (FPM, SPM, HPM, and VPM) do not include drift due to yaw of repose and correspondingly suffer in cross-range error to within less than about 20 m of each other. As $T^* \rightarrow 1$, the point mass IPPs converge to the correct cross-range location due to a shorter trajectory prediction containing less drift effect.

The radial impact error is a simple root sum square of the results in Figs. 3(a and b). MLT improves in radial impact prediction error from about 25 m at $T^*=0$ to less than 1 m at $T^*=1$. The coning motion near the end of the flight, however, increases the MLT estimate above all other IPPs studied at some point. The radial impact estimation for MPM increases to about 20 m (mainly in the down-range direction) near apogee. Radials errors for FPM and SPM IPPs vary from over 120 m at $T^*=0$ to less than 10 m at $T^*=0.8$ due to improvement in the cross-range prediction. While both the HPM and VPM IPPs have over 150 m of radial error at $T^*=0.6$, the results asymptote to less than 5 m of radial error by $T^*=0.9$. A steeper quadrant elevation trajectory was also examined. The baseline 6DOF was exercised at 45° quadrant elevation with a muzzle velocity of 656.8 m/s and muzzle spin rate of 1332.0 rad/s. Launch disturbances $(\tilde{v},\tilde{w},\tilde{q},\tilde{r})$ were again zero.

The flight dynamics at 45° quadrant elevation are shown in Fig. 4. The projectile flew over 17 km down-range, climbed to almost 6 km in altitude, and drifted in the cross-range direction by over 400 m. This flight also spanned supersonic to transonic Mach numbers. A larger yaw of repose and a more active limit cycle are seen in Fig. 4(c). For this larger quadrant elevation flight, the coning motion of approximately 3° total angle of attack occurs for about the final 50% of the flight.

The IPP algorithms were performed for the 45° flight in a manner similar to the 20° flight. The results of the impact point prediction errors in the down-range, cross-range, and radial direc-

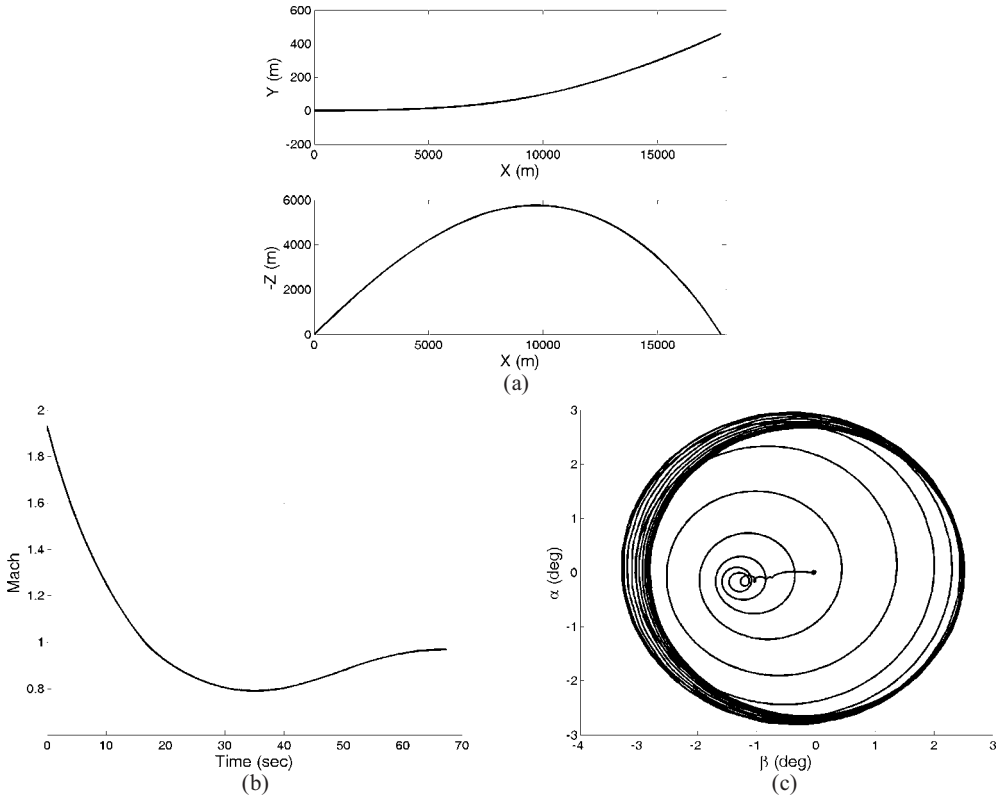

Fig. 4. Flight dynamics of the artillery projectile at 45° quadrant elevation: (a) trajectory; (b) Mach number history; and (c) angle of attack behavior

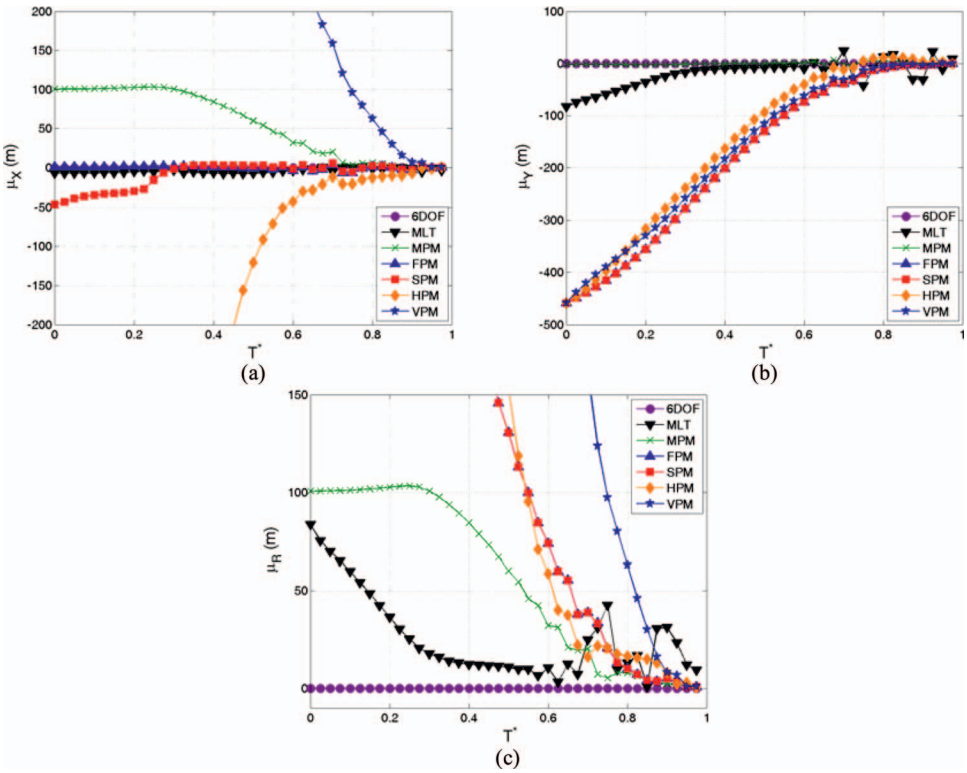

Fig. 5. (Color) Mean of impact point prediction for 45° quadrant elevation and perfect parameters and initial states: (a) down-range direction; (b) cross-range direction; and (c) radial direction

tions as a function of normalized time of flight are given in Fig. 5. Again, the 6DOF model has zero model errors as seen in Fig. 5

MLT predicts down-range impact to within 10 m throughout the flight as shown in Fig. 5(a). Down-range impact is overpredicted by MPM by about 100 m from $T^*=0$ to about $T^*=0.3$. Overestimation of down-range impact suggests a source term in the MPM equations of motion. It may be possible to account for this overprediction in down range by some scaling of the axial force aerodynamic coefficient. Over the entire flight, the FPM predicts down-range impact to within 10 m. The SPM initially underpredicts down-range impact by about 50 m; however, by about $T^*=0.3$ the error is less than 10 m. It is possible that the projectile has crossed some critical altitude or Mach regime that improves the SPM estimate. Down-range estimates from HPM (underprediction) and VPM (overprediction) are qualitatively similar to the 20° case. In general, for all IPPs throughout the entire flight, the down-range impact predictions defy general trends. All IPP results are nonsmooth for $T^*>0.5$, implying that the limit cycle negatively influences each IPP.

Fig. 5(b) presents cross-range prediction errors for the 45° quadrant elevation and no parameter or state errors. Similarly to the 20° results, the IPP algorithms are grouped between equations of motion that address drift and those that do not. The MPM cross-range estimate is within about 5 m for the whole flight. MLT estimates of cross-range impact monotonically decrease from about 85 m at launch to less than 10 m at $T^*=0.5$ before the limit cycle produces the erratic results seen for $T^*>0.5$. The FPM, SPM, HPM, and VPM have about 450 m of cross-range error and decrease to within 5 m by $T^*=0.9$.

Radial impact errors in Fig. 5(c) show that for $T^*<0.5$ the order of IPP preference based solely on model errors for this case would be (from first to last) 6DOF, MLT, MPM, FPM, SPM, HPM, then VPM. Coning motion evident in the angle of attack of Fig. 4(c) for $T^*>0.5$, however, complicates this picture. The limit cycle clearly degrades MLT performance in Fig. 5(c) for $T^*>0.5$; for most instances MLT features the highest radial impact prediction error. Irregular radial prediction curves for MPM, FPM, SPM, and HPM for $T^*>0.5$ indicate that the coning motion induces erroneous impact point predictions in these IPPs as well. These IPPs are less dependent on the angular motion, however, due to simpler equations of motion.

In reality, the state and parameters cannot be known exactly. State errors result from measurement and subsequent processing in the state estimation process. The magnitude of state errors depends on the sensor type and processing technique used for a specific application. One standard deviation of initial state errors used in this effort is provided in Table 3. Bias errors are constant for a given flight and random errors occur whenever a new state estimate is obtained during the flight. These nominal values were also multiplied by a factor of 2 to identify the dependence of each IPP on initial state error magnitude.

Uncertainty was also placed on the projectile parameters. Error in projectile parameters accounts for measurement error and manufacturing tolerances. For example, aerodynamic coefficients can only be inferred from spark range testing to a certain degree of accuracy. Uncertainty also accompanies measurement of physical parameters such as mass and inertia. Furthermore, measurement sample size constraints may prevent a fully representative characterization of manufacturing variability. Test data resident at the Army Research Laboratory were used to determine the magnitude of projectile parameter errors. These distributions, given as one standard deviation in Table 4, were applied as a bias error in the IPP assessments.

Table 3. Nominal Initial State Errors ($1-\sigma$)

State	Bias	Random
Down-range (X) inertial position (m)	1.0	1.0
Cross-range (Y) inertial position (m)	1.0	1.0
Altitude (Z) inertial position (m)	1.0	1.0
Pitch inertial orientation (deg)	1.0	1.0
Yaw inertial orientation (deg)	1.0	1.0
Roll inertial orientation (deg)	1.0	1.0
Body X velocity (m/s)	0.1	0.1
Body Y velocity (m/s)	0.1	0.1
Body Z velocity (m/s)	0.1	0.1
Body X angular rate (deg/s)	1.0	1.0
Body Y angular rate (deg/s)	1.0	1.0
Body Z angular rate (deg/s)	1.0	1.0

The Monte Carlo evaluation simulated 1,000 shots. All errors (states and parameters) were assumed normally distributed. The states and parameters from the baseline 6DOF were corrupted with bias and random errors before running the IPP algorithms. Bias errors were held constant for a given shot and random errors were reevaluated at each point along the trajectory where the IPP algorithms were exercised. The errors were used similarly for each IPP to ensure consistency. The impact point predictions from each IPP were used to calculate the mean and standard deviation of the down-range, cross-range, and radial direction difference from the nominal impact point. The mean impact point prediction with nominal parameter and initial state errors yields the overall accuracy of the IPP while the standard deviation of the impact point prediction illustrates the variability in IPP accuracy.

The mean impact point prediction for each IPP with a 45° quadrant elevation is presented in Fig. 6. The 6DOF, MLT, and FPM IPPs exhibit similar down-range performance for the nominal parameter and state errors. These three IPPs overpredict down-range impact by about 100 m at $T^*=0$ and improve to less than 10-m error past $T^*=0.6$. SPM predicts shorter range than the 6DOF, MLT, and FPM until about $T^*=0.3$, where the results become similar to these three IPPs. Down-range impact is overestimated by MPM by about 200 m at $T^*=0$ and does not get within 10 m until about $T^*=0.7$. The HPM IPP underpredicts range before closing to within 10 m around $T^*=0.8$. As expected, the VPM overpredicts range due to neglecting aerodynamics. The magnitude of the mean down-range impact for all IPPs agrees to

Table 4. Parameter Errors ($1-\sigma$)

Projectile parameter	Errors
Mass (kg)	0.1451
Diameter (m)	0.0001807
Axial inertia (kg-m^2)	0.0005870
Transverse inertia (kg-m^2)	0.01975
CG location (m)	0.001288
Axial force (%)	1
Normal force (%)	5
Magnus force (%)	25
Roll damping moment (%)	5
Pitching moment (%)	2
Pitch damping moment (%)	15
Magnus moment (%)	15

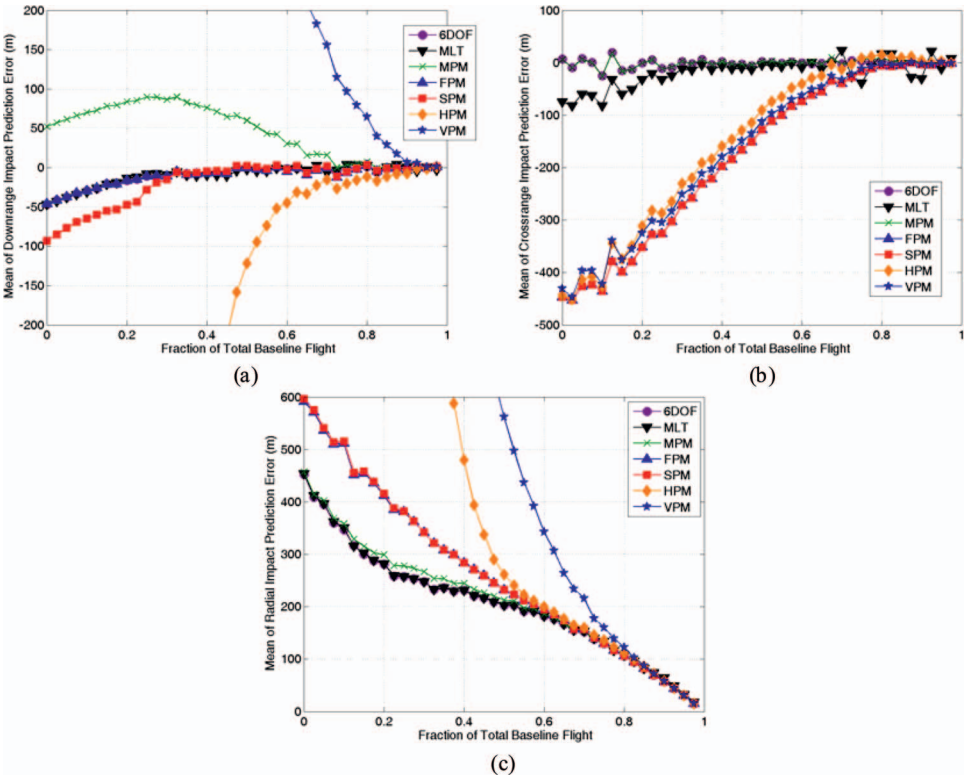

Fig. 6. (Color) Mean of impact point prediction for 45° quadrant elevation and nominal parameter and initial state errors: (a) down-range direction; (b) cross-range direction; and (c) radial direction

within the statistical uncertainty with the model only results presented in Fig. 5, with the exception of a general overprediction for $T^* < 0.2$.

The mean of cross-range predictions for the model only [Fig. 5(b)] and the nominal parameter and state error [Fig. 6(b)] cases is also similar. Results are separated into IPPs that account for drift (6DOF, MLT, and MPM) and those that do not (FPM, SPM, HPM, and VPM). There is about 100 m of scatter in the data for $T^* < 0.2$. All IPPs are within 10 m by $T^* = 0.8$ with the exception of the MLT which exhibits about 20–30 m of spread.

The data shown in Fig. 6(c) are not simply the root sum square of the results in Figs. 6(a and b). Fig. 6(c) is the mean of the root sum square of the down-range and cross-range impact point for an individual Monte Carlo trial. The mean radial impact prediction error is about 400 m for the 6DOF and MLT IPPs at $T^* = 0$. The 6DOF and MLT radial prediction errors decrease to about 100 m at $T^* = 0.8$. The MPM, FPM, SPM, HPM, and VPM IPPs have higher radial prediction errors and each gradually converges to the result for the 6DOF as time increases (MPM at $T^* = 0.5$, FPM and SPM at $T^* = 0.6$, HPM at $T^* = 0.65$, and VPM at 0.85). The MLT estimates remain about 5–10 m larger than all other IPPs for $0.88 < T^* < 0.98$. Comparing Fig. 5(c) with Fig. 6(c) indicates that the impact point errors induced by the propagation of erroneous parameters and states through the IPP algorithms are larger than the model only errors for this set of parameter and state errors.

The standard deviation of the impact point prediction for each IPP is shown in Fig. 7 for the nominal parameter and initial state errors. The magnitude of the standard deviation in the down-range direction is similar for all IPPs. A humped shape is evident in Fig. 7(a), possibly corresponding to apogee of the baseline trajectory. The down-range standard deviation decreases to about 50 m at $T^* = 0.9$. The standard deviation in the cross-range direction for all IPPs is larger than the down-range direction for $T^* < 0.5$. Past $T^* = 0.5$, the magnitude of the cross-range standard deviation is similar for all IPPs and reduces to about 30 m at $T^* = 0.9$. Radial standard deviations in Fig. 7(c) range from about 350 m (FPM and SPM) to 100 m (VPM) at $T^* = 0$. Results generally reduce as T^* increases and suggest a radial standard deviation of approximately 30 m for all IPPs at $T^* = 0.9$.

The mean of the impact point prediction for each IPP is shown in Fig. 8 for the twice nominal parameter and initial state error level. Down-range and cross-range mean impact prediction error magnitude agrees with those for the nominal parameter and state errors shown in Figs. 6(a and b). The only exception to this finding is for mean down-range predictions for $T^* < 0.5$. The nominal error level overpredicts while the twice nominal results suggest a general underprediction. Qualitative agreement is also apparent in mean radial prediction errors between nominal error levels [Fig. 6(c)] and twice nominal error levels [Fig. 8(a)]. Comparing the magnitudes of these results indicates that the mean radial impact error scales linearly with the parameter and state error. For example, at $T^* = 0.8$ all IPPs show a radial impact error of about 100 m for the nominal errors and about 200 m for the twice nominal errors.

The standard deviation of the impact point prediction for each IPP is shown in Fig. 9 for the twice nominal parameter and initial state errors. The trends in the curves in Fig. 9 match those for the nominal error level in Fig. 7. Similar to the finding for the relationship between means for the nominal and twice nominal error level, the standard deviations seem to scale linearly with the input error levels. The standard deviation of the radial error at 0.9 is about 30 m for the nominal errors and about 60 m for the twice nominal error level shown in Fig. 9(c).

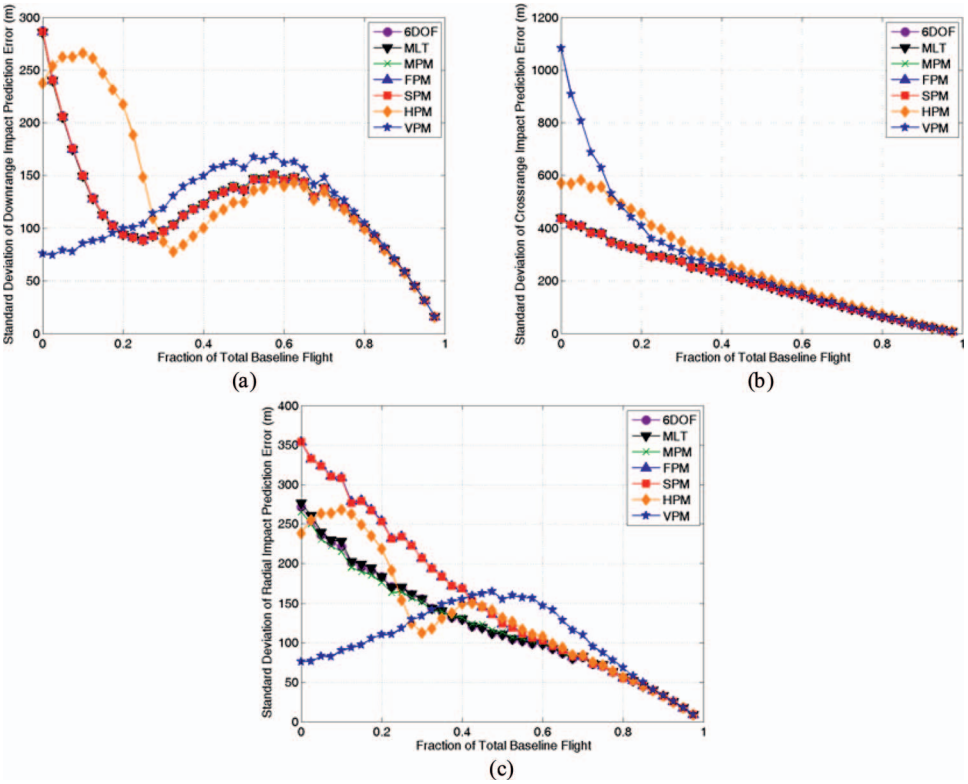

Fig. 7. (Color) Standard deviation of impact point prediction for 45° quadrant elevation and nominal parameter and initial state errors: (a) down-range direction; (b) cross-range direction; and (c) radial direction

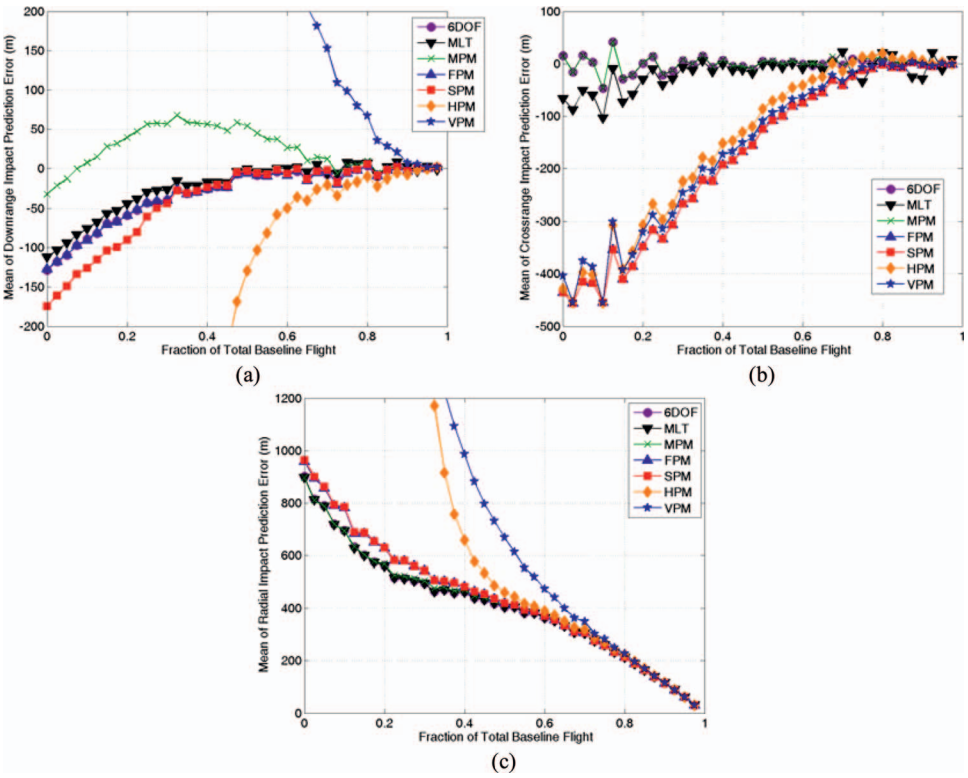

Fig. 8. (Color) Mean of impact point prediction for 45° quadrant elevation and twice nominal parameter and initial state errors: (a) down-range direction; (b) cross-range direction; and (c) radial direction

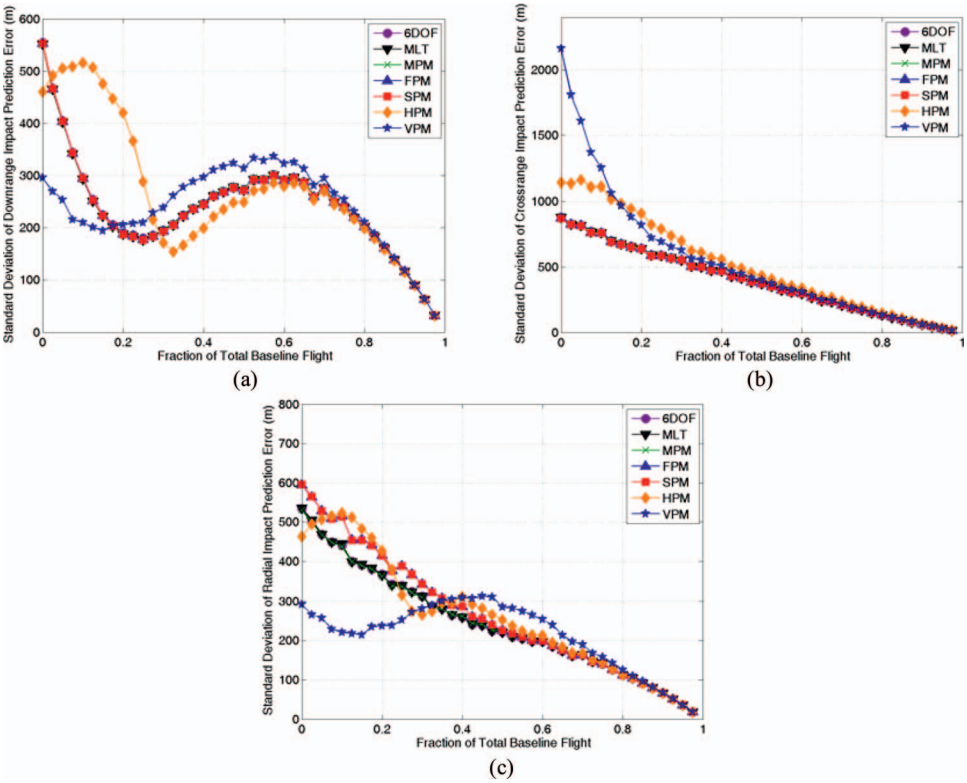

Fig. 9. (Color) Standard deviation of impact point prediction for 45° quadrant elevation and twice nominal parameter and initial state errors: (a) down-range direction; (b) cross-range direction; and (c) radial direction

Conclusions

IPPs are used in the guidance and control of gun launched smart munitions. The optimal IPP for a given application or family of systems is currently unknown. Seven IPPs were developed in this effort. These IPPs were applied to a 20° and 45° quadrant elevation flight of a 155-mm artillery projectile.

The investigation of model error illustrated that neglecting critical physics in the equations of motion can result in poor impact point prediction. The 6DOF, as the truth model, was assumed to have no model errors. MLT was shown to have low model error (<20 m) for most of the flight, except for times during which a limit cycle is active. Cross-range predictions of the MPM were highly accurate (<5 m), but down-range impact was generally overpredicted by the MPM. This suggests some scaling of the axial force aerodynamic coefficient to resolve a potential source term in the MPM equations of motion. There was little difference between the FPM and SPM IPPs, indicating that updating the atmospheric density and axial force aerodynamic coefficient was not of significant value in this specific scenario. FPM and SPM featured good down-range performance (usually within 20 m) balanced by poor cross-range impact prediction since yaw of repose is not included in the dynamic model. The HPM and VPM IPPs also neglect yaw of repose and consequently suffer in cross-range performance. Down-range impact is underpredicted by the HPM and overpredicted by the VPM IPPs. All IPPs converge to the true impact point as the time of estimation approaches the time of impact. The coning motion, due to a nonlinear Magnus moment, adversely affects all IPPs and the MLT appears the most sensitive.

In practice, state estimation, physical properties, and aerodynamics possess some uncertainty. These effects were included through a parameterization. A limited set of Monte Carlo trials were conducted to assess IPP performance with state and parameter errors. The down-range and cross-range impact trends for the state and parameter error cases were similar to the model only case for all IPPs. The magnitudes of the radial impact errors were often higher by one order of magnitude or more for the state and parameter error cases than the model only case. This indicates that propagation of incorrect states and parameters at these levels through the IPP algorithms dominates the model errors. The impact point errors scale linearly with the state and parameter errors. For this reason, global positioning system or inertial measurement unit errors or uncertainty in the aerodynamics or physical properties directly relate to the IPP performance. The impact point performance with the state and parameter errors was insensitive to IPP type for $T^* > 0.8$. The control authority available and time of flight at which course corrections take place may determine the optimal IPP for a given application. For example, if much control authority was available late in flight ($T^* = 0.9$) then a 6DOF IPP is no better than a VPM IPP. If small maneuvers are only possible early in flight then a 6DOF, MLT, or MPM IPP may be required.

Notation

The following symbols are used in this paper:

C_{DD} = roll moment aerodynamic coefficient due to fin cant;
C_{LP} = roll damping aerodynamic coefficient;
C_{MA} = pitch moment aerodynamic coefficient;
C_{MQ} = pitch damping aerodynamic coefficient;
C_{NA} = normal force aerodynamic coefficient;
C_{NPA} = Magnus moment aerodynamic coefficient;
C_{X0} = zero yaw axial force aerodynamic coefficient;

C_{X2} = yaw angle squared axial force aerodynamic coefficient;
C_{YPA} = Magnus force aerodynamic coefficient;
CG = center of gravity;
c = speed of sound;
D = projectile reference diameter;
g = acceleration of gravity;
h_a = $h_L^2/(1-h_M)-h_M$;
h_L = $I_{XX}(C_{NA}-C_{X0})/mD^2C_{MA}(\dot{\phi}D/V)$;
h_M = $=I_{XX}C_{NPA}/mD^2C_{MA}(\dot{\phi}D/2V)^2$;
I = projectile inertia matrix;
I_{XX}, I_{YY}, I_{ZZ} = diagonal components of inertia matrix;
I_{XY}, I_{YZ}, I_{XZ} = off-diagonal components of inertia matrix;
$\tilde{L}, \tilde{M}, \tilde{N}$ = external moments on projectile, expressed in no-roll frame;
m = mass of projectile;
$\tilde{p}, \tilde{q}, \tilde{r}$ = projectile roll, pitch and yaw rates, expressed in no-roll frame;
R_{MCM} = distance from center of mass to Magnus center of pressure along station line;
R_{MCP} = distance from center of mass to center of pressure along station line;
s = dimensionless arc length;
T^* = normalized time;
t = time;
t_{go} = time to go;
$\tilde{u}, \tilde{v}, \tilde{w}$ = projectile velocity components expressed in no-roll frame;
V = total velocity;
$\tilde{X}, \tilde{Y}, \tilde{Z}$ = external forces on projectile expressed in no-roll frame;
x, y, z = projectile position in inertial space;
x_i, y_i = impact position in x and y coordinates;
α, β = aerodynamic angles of attack in pitch and yaw planes;
α_r = yaw of repose;
θ_v, ψ_v = projectile heading angles;
μ_X, μ_Y, μ_R = mean of impact point prediction error in down-range, cross-range, and radial directions;
ρ = atmospheric density;
$\sigma_X, \sigma_Y, \sigma_R$ = standard deviation of impact point prediction error in down-range, cross-range, and radial directions; and
ϕ, θ, ψ = projectile roll, pitch and yaw angles.

References

Burchett, B., and Costello, M. (2002). "Model predictive lateral pulse jet control of an atmospheric rocket." *J. Guid. Control Dyn.*, 25(5), 860–867.

Cooper, G. R., Fansler, K. S., and Oskay, V. (1997). "Extracting meteorological data from projectile trajectory." *J. Spacecr. Rockets*, 34(6), 769–773.

Hainz, L., and Costello, M. (2005). "Modified projectile linear theory for rapid trajectory prediction." *J. Guid. Control Dyn.*, 28(5), 1006–1014.

Lieske, R. F., and Reiter, M. L. (1966). "Equations of motion for a modified point mass trajectory." *U.S. Army Ballistic Research Laboratory Rep. No. R1314 (AD 485869)*, U.S. Army, Aberdeen Proving Ground, Md.

McCoy, R. L. (1999). *Modern exterior ballistics: The launch and flight dynamics of symmetric projectiles*, Schiffer Publishing, Atglen, Pa.